# Electrochemical Performance Enhancement Zinc Cobaltite-Reduced Graphene Oxide for Next Generation Energy Storage Applications



# Electrochemical Performance Enhancement Zinc Cobaltite-Reduced Graphene Oxide for Next Generation Energy Storage Applications

**Noor Hussien AbdAli[1], Shaymaa Hadi Al- Rubaye[2], Bahaa H rabee[2], Kalid Haneen Abass[2]**

[1]Babylon Education Office
[2] Department of Physics, College of Education for Pure Sciences, University of Babylon, Iraq.

Corresponding author E-mail: pure.shyma@uobabylon.edu.iq

**Abstract.** Recently, metal oxide decorated reduced graphene oxide based nanosheets have gained much attention because of their widespread applications in electrochemical energy storage devices, particularly in supercapacitors. Motivated by this, in the present study, zinc cobaltite-reduced graphene oxide $ZnCo_2O_4$-rGO (reduced graphene) nanoporous arrays were developed directly on a Ni foam piece by using a specific hydrothermal method, which is simple, cost-effective, and facile and followed by a process for annealing purpose. The nanocomposite of the as-prepared $ZnCo_2O_4$-rGO involves $ZnCo_2O_4$ wrapped in conducting rGO sheets in order to maintain short distance for the ion diffusion process, stable structural integrity, and pathways for percolating electron conducting. As a result, this nanocomposites displays an impressive overall electrochemical performance, such as a promising capacitance (1242 F g-1 )at a current density of 2 A g-1) and remarkable cycling stability (92% capacitance retention after 10000 charge-discharge cycles at 2 A g-1). The device showed highest energy density of ~32W h kg−1 at a power density of 1252 W kg−1The feasible design presented in this paper delivers a good synergism between the $ZnCo_2O_4$ and rGO that providing superior electrochemical performance.

## 1. Introduction

Recently, the concern about the environmental pollution and the fossil fuels depletion is increased and is going to do so in the future. So that, a crucial requirement for alternative sources of an efficient, clean, and a suitable energy source for energy storage is emerged for maintaining a rapid and healthy economic development. The supercapacitors (SCs) and the Lithum-ion batteries are considered as the most important devices used for storing the electrical energy. They got the attention of a lot of researchers in this filed due to its superior characteristics. Particular speaking, researchers have put much more attention on the supercapacitor's energy storage due to its outstanding characteristics, such as its long life cycle, fastest ability for recharging, higher performance, and low cost for operating and maintenance [1,2]. These batteries have been used for widespread applications that require a steadily source of energy, such as the batteries that used in the hybrid and pure electrical cars and other mobile electronic devices, etc. [3,4]. In addition, the supercapacitor's batteries are used as a complement or alternative energy storage in the applications that require higher power uptake and delivery. The supercapacitors, in general, can be classified into two types regarding energy

storage mechanism, ion adsorption (double-layer electrochemical capacitors) and the fast surface redox reaction (pseudocapacitors).

The second type (pseudocapacitors) provides a higher level of energy as compared to the first type of these capacitors [5]. Due to the superior characteristics of the pseudocapacitors, a lot of researches have been studied this type of batteries for getting a better understanding and gain a higher performance. Metal sulphide, metal oxide, and conductive polymers have been introduced as new materials for designing and developing batteries with longer cycle life and higher level of energy storages. In addition, novel materials with high specific surface have been extensively developed and that is because the capacitance of the storage is basically determined by the reaction of the surface redox of the active materials. $ZnCo_2O_4$ is considered as one of the most promising and outstanding functional materials that used, and is going to be used in the future, for various electrochemical applications, such as supercapacitor, electrocatalysis, and Li-ion batteries due to its rich redox reactions and the higher level of its electrochemical activity [6]. In addition, $ZnCo_2O_4$ shows a great electrochemical activity (theoretical capacitance, ~2604 $Fg^{-1}$) and that makes it superior for the electrical application [7]. In the present study, we prepared $ZnCo_2O_4$-rGO nanoporous composite using a hydrothermal technique followed by heat treatment (pristine $ZnCo_2O_4$ SEM images and $ZnCo_2O_4$-rGO are provided in Figure 2). The as-prepared composite sample possessed an ultrahigh specific capacitance of 1242 $Fg^{-1}$ at a 2 $Ag^{-1}$ current density in 2 M KOH solution.

Furthermore, the 3D electrode showed a great electrochemical performance, such as the outstanding cyclic stability (~92% as the ratio of the capacitance retention after 10000 cycles). Effects of concentration of the electrolyte on the $ZnCo_2O_4$-rGO electrical performance were examined as well. $ZnCo_2O_4$-rGO composite material with this remarkable electrochemical performance can be considered as a potential and an alternative candidate for achieving high performance applications of the supercapacitor.

## 2. Experimental Techniques

### *2.1. Chemicals*

A naturally grown flake of graphite of 150 μm (99.9% purity) particle size was purchased from Aldrich. The other chemical materials that used in this work (analytical grade), are provided by Sigma Aldrich and required no additional purification.

### *2.2. Synthesis of graphene oxide (GO)*

To synthesize GO, the modified Hummers method is used [8]. In the classical procedure, 23 ml of the $H_2SO_4$ (98%) was mixed with 1 g of the naturally grown graphite flake in a round-bottom flask. Then, the mixture stirring vigorously in an ice bath. Next, only 3 g of $KMnO_4$ was carefully and wisely added at an accurate controlled rate. Next, the resulted mixture was enforcedly stirred for 2 hours provided maintaining the reaction temperature less than 5 ºC. Next, the whole mixture immersed in preheated path of oil and continued to act at 35ºC for 6 hours. Next, 45 ml of DI was added to the mixture and the resulted mixture stirred together for another 2 hours. After the stirring process got done, the resulted mixture was placed in a beaker of 5L in capacity. Amount of 35% of the $H_2O_2$ was slowly added until the whole mixture turned yellow. Dilute HCL solution (measured by 5% by volume) was then added for removing the residual of the manganese salt. It worth to mention that the resulted GO suspension yielded a brown dispersion. Finally, distilled water was used in order to wash the GO for several times for getting neutral dispersion pH.

### *2.3 Preparation of ZnCo2O4 – rGO (ZCO-rGO) nanocomposite*

A hydrothermal method is used for synthesizing the The ZCO-rGO nanocomposite. Several steps is involved in the synthesis: In a typical experiment, the substrate of the Ni foam, 2 x 0.1 cm in dimensions, degreased by using acetone. Then, the substrate was cleaned and etched by

using 4 M HCL in an ultrasound environment for 20 minutes in order to remove the surface layer of NiO and then rinsed by DI and absolute ethanol for 30 minutes, respectively. For the hydrothermal method, $Zn(NO_3)_2 \cdot 6H_2O$ (0.595 g) and $Co(NO_3)_2 \cdot 6H_2O$ (1.164 g) were melted (dissolved) discretely in 30 mL of DI along with magnetic stirring. Simultaneously, $Co(NH_2)_2$ (0.601 g) and $NH_4F$ (0.148 g) were dissolved in mixture contains 20 mL for both of ethanol and ID with magnetic stirring. The stirring process lasted for 30 minutes. Then, a solution of zinc nitrate was added slowly to the solution of cobalt nitrate. Next, the mixture of urea and ammonium fluoride added to cobalt and zinc nitrates mixture along woth magnetic stirring at RT for 30 minutes. Then, the resulted mixture was places in a Teflon-lined autoclave manufactured from stainless steel of 100 mL in volume. The reaction was accomplished for 24 hours and maintained at 120 ºC. as soon as the reaction completed, the autoclave left to be cooled at RT. DI was used to wash the resulted product for several times followed by ethanol as well. After that, the product was dried in a vacuum maintained at 80 ºC and lasted for 8 hours. The resulted product was calcined for 2 hours at 400 ºC and atmosphere with 2 ºC $min^{-1}$ as the ramping rate by using a programmable and controllable furnace to get the final product of the composite NCO-rGO. The original (pistine) ZCO was produced similarly . However, GO was not added.

### *2.4. Phase, morphology, and electrochemical characterizations*

The phase formation, features of the crystalline, and the morphology of the synthesized samples were examined by using the XRD, GBC MMA XRD, field emission scanning electron microscopy (FESEM, JEOL JSM-7500FA), high resolution transmission electron microscopy (HR-TEM, model: JEOL JEM-2011), Raman spectroscopy (JY HR800 Spectrometer), and X-ray photoelectron spectroscopy (XPS,SPECS GmbH). Studies that related to the gas adsorption were obtained by using calculations of Brunauer-Emmett-Teller (BET). Distributions of pore size were obtained by using the NLDFT slit-cylinder pore equilibrium model for $N_2$ at 77 K as accomplished in the Quantachrome software (v 3.0).

### *2.5. Electrochemical measurements*

The ZCO-rGO and ZCOelectrochemical tests were conducted by three electrode system in the electrolyte of 2 M KOH. Hg/HgO electrodes and Pt mesh were used as the reference and the counter electrode, respectively. Mixing the active materials (80%) of (ZCO-rGO or ZCO), (10%) from acetylene black, and (10%) of polyvinylidene fluoride (PVDF) binder and all together in N-methyl-2-pyrrolidinone (NMP) solvent. Subsequently, the final mixture had been blended overnight, loading the slurry onto the nickel foam having area of 1.0 cm × 1.0 cm and drying it under vacuum for 10 h at 80 ºC. a pressure of 4 MPa had been used to press the electrode and leaving it to dry overnight. Utilizing a digital scale with an accuracy equals to 0.01 mg, the active material mass loading was obtained via measuring the Ni foam prior and after material coating. The electroactive substance, provided by nickel (Ni) foam with 1 $cm^2$ in area, had been utilized directly as the working electrode. The ZCO-rGO's mass loading on the Ni foam of 0.86 $mg/cm^2$ was used. Measurements of cyclic voltammetry (CV) had been conducted in an electrochemical workstation (CHI660B, Chenhua, Shanghai) within the range of potential equals to 0−0.45 V (Hg/HgO) at various rates of scanning. The galvanostatic charging-discharging tests had been performed on a testing system of controlled program LAND battery. Measurement (CHI660B) of electrochemical impedance spectroscopy (EIS) was conducted using an AC voltage of 5 mV in amplitude over a frequency bandwidth ranged from 0.01 to 100 kHz at open circuit potential.

The electrode's specific capacitance (C) in ($Fg^{-1}$), from the CV, was calculated as per equation (1) [9].

$$C = \frac{\int Idv}{mv\Delta V} \quad (1)$$

Where *m* denotes to the active material mass (g), *I* denotes to the voltametric current (A), $\Delta V$ denotes to the CV's potential window (V), and ν is the rate of scanning. Therefore, equation (1) could be rewritten as:

$$C = \frac{I\Delta t}{m\Delta V} \quad (2)$$

Where Δt refers to time of discharging, *I* denotes to the discharging current, and *m* is the active material's total mass. The specific energy (*E*) in W h $kg^{-1}$ and the specific power (P) in W $kg^{-1}$ could be obtained from using equations (3 and 4) [9].

$$E = \frac{0.5C(\Delta V)^2}{3.6} \quad (3)$$

$$P = \frac{E3600}{\Delta t} \quad (4)$$

## 3. Results and discussion

Figure Figure 1 exhibits the patterns of XRD of ZCO (pure) and the ZCO-rGO composites. The patterns of XRD of both materials exhibited high diffraction intensity peaks (DIPs) represented by (111), (220), (311), (400), (422), (511), and (440) planes. All the well-defined diffraction intensity peaks could be easily indexed to the spinel crystalline structure of ZnCo2O4 (JCPDS Card no. 23-1390, space group Fd3m). There is no observation of other clear peaks in the pattern of XRD. Consequently, it confirms that the predecessor has been entirely converted into spinel ZnCo2O4 after the process of annealing. Furthermore, the relatively high DIPs indicate that the porous $ZnCo_2O_4$ (as-prepared) is highly crystalline.

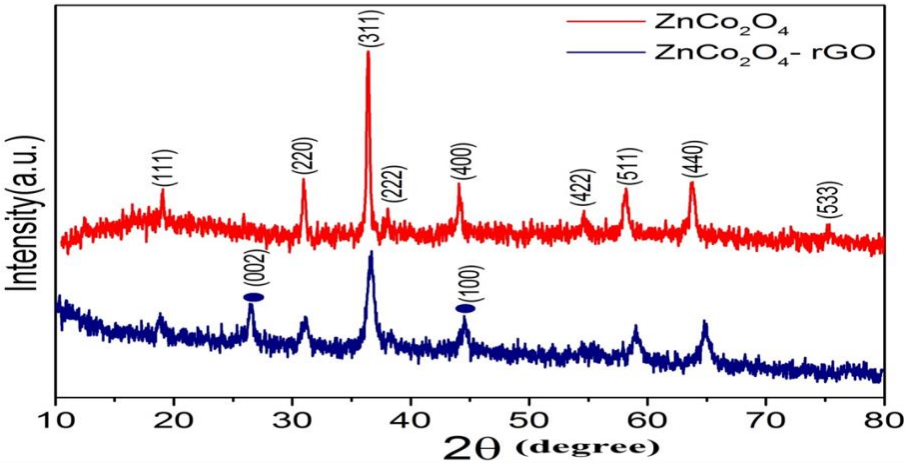


**Figure 1.** XRD patterns of pure ZCO and ZCO-rGO nanocomposite.

the graphite XRD's spectrum showed a peak (002) with strong characteristics. After performing the processes of oxidation and exfoliation, the (002) peak vanished and another new peak has appeared at ~45.60°, representing the (100) GO's planes, which reveals the conversion of graphite to GO.

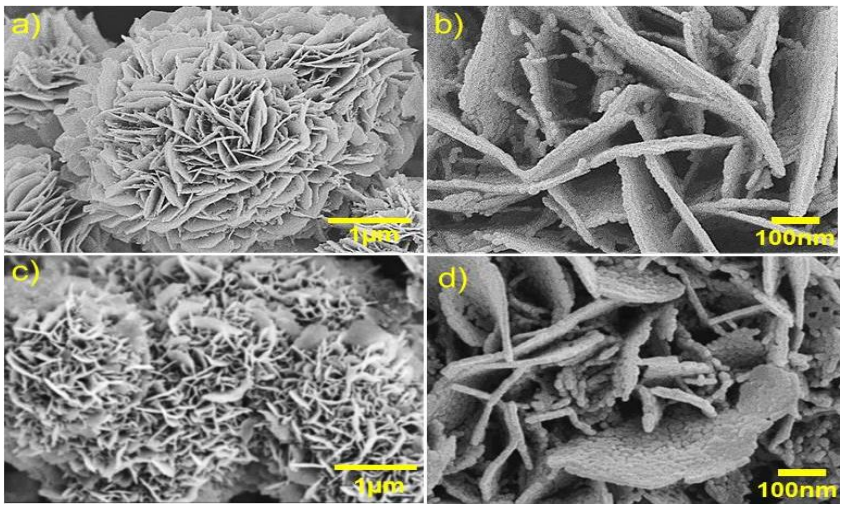


**Figure 2.** SEM images at different magnification (a, b) of the ZCO nanoporous and (c, d) of the ZCO- rGO nanocomposites.

The $ZnCo_2O_4$ nanoporous microstructure and its morphology were examined by TEM and SEM tests. The typical SEM images at different magnification are shown in Figure 2 with different magnifications. There are many of individual microspheres that take a 3D flower shape similar consist of hierarchical assemblies of interconnected nanoflakes that are aligned by the edges of the surface. These samples showed a regular flower like-nanoflakes with some irregularity in the nanostructure features at the surface. Additionally, the ZCO-rGO images showed the nanoflakes are constructed by stacking multi sequential layers that was not noticed in the pure ZCO.

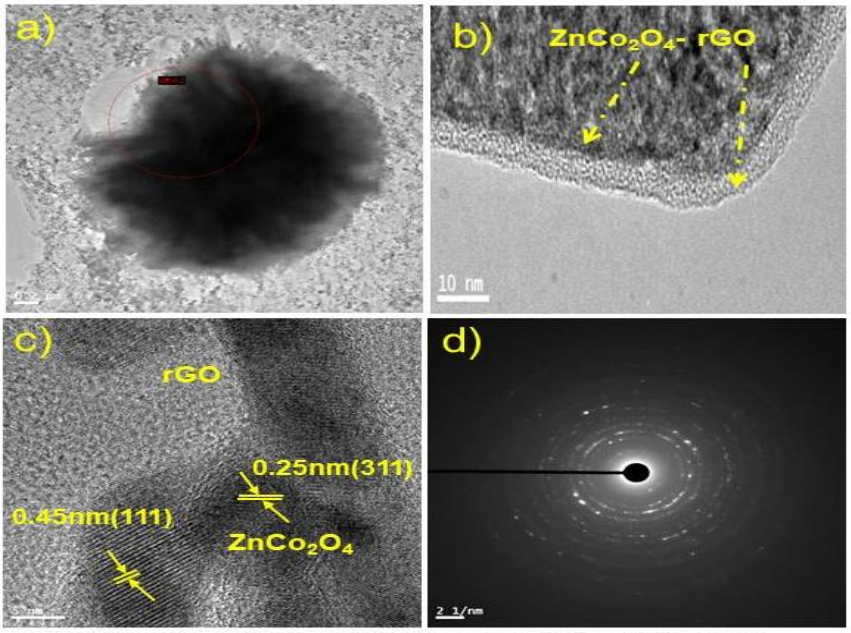


**Figure 3.** The sub figures (a, b, c) represent different magnifications of TEM images for ZCO-rGO. (d) the electron diffraction pattern of the selected area.

The morphology of the ZCO and typical ZCO-rGO nanoflakes were further analyzed using TEM and HRTEM (Figure 3 (a-d)). Figure 3 (a) displays a TEM image of pristine ZCO. The morphology of the surface shows the pores existence. Latest studies in this field have indicate that structures of porous were formed within the materials pores of the electrode that could work as an electrolyte ion reservoir [10]. This will offer electrolyte's spatial confining and get a close contact between the electrolyte and the material of electrode along with ensure a stable provide of electrolyte ions [11]. Therefore, the structure of the porous has the ability of better providing the interaction between electrolyte/electrode and enabling the electrochemical reactions. Figure 3 (b) shows the ZCO-rGO TEM image, in which the existence of rGO (1.7 nm) thin layered on ZCO as a coating is very obvious. The HRTEM image in Figure 3 (c) exhibits the complete contact between the ZCO porous structure and rGO, which is the main reason behind the electronic conductivity improvement of the ZCO-rGO system. There are also a set of distinct parallel fringes having 0.25 nm of d-spacing for the planes (311) and 0.45 nm denoting the planes (111). Figure 3 (d) refers to the electron diffraction pattern of the selected area, that shows the crystalline's feature of the nanoporous ZCO. This pattern of diffracting electron consists of the well-defined rings that are easy to index to the ZCO's spinel planes of (111, 220, 311, 400, 422, 440, and 511).Compared to the pristine ZCO sample, the well-wrapped ZCO-rGO structure appears electrochemically more active. The rGO coating might be useful for electrons and ions to be easily accessed to the active surfaces, allowing for a rapid conversion reaction that leads to improve the performance of the power. Moreover, as the rGO layers could function like a mechanical shield, any big variation in the ZCO volume could be accommodated without insolating the particle from the layers of rGO. This will contribute in improving the cycling performance [12].

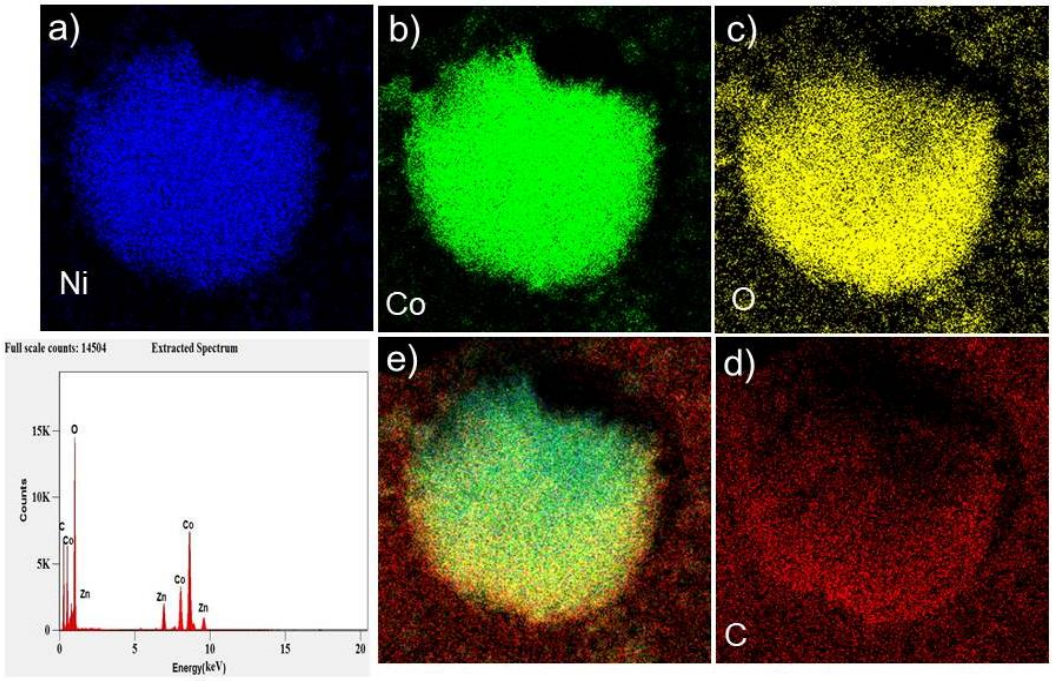


**Figure 4.** Elemental mapping of ZCO-rGO showing the existence of (a) Nickel, (b cobalt (c) oxygen, (d) carbon and e) EDS spectrum showing peaks of Ni, Co and O with carbon

Figure 4 also shows the associated elemental mapping of the energy dispersive spectroscopy (EDS). It provides sufficient information regarding to the elements' distribution within the nanoflakes. It, therefore, confirms the well wrapping of ZCO structure by the layered rGO and

clearly displays the presence of uniform and thin-layered of the carbon coating over the ZCO hexagon for the ZCO-rGO system (Figure 4e)

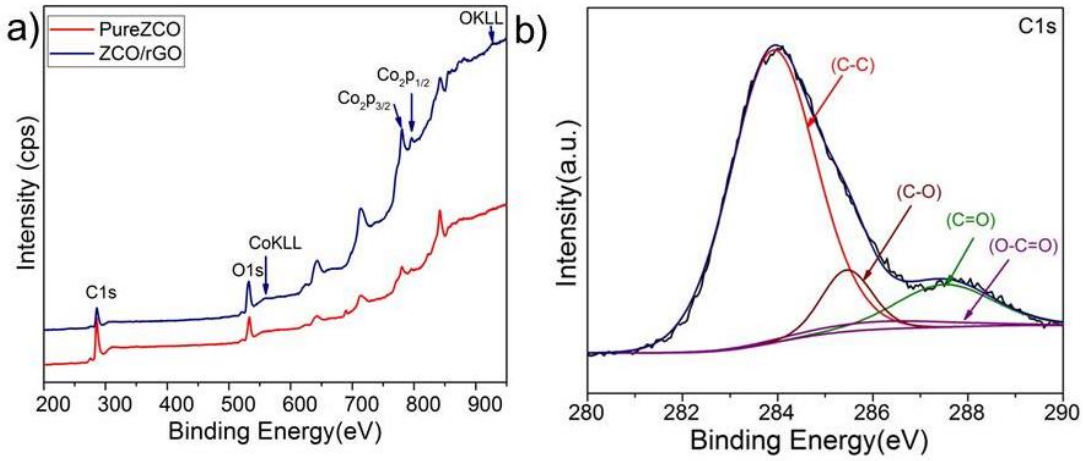


**Figure 5.** XPS spectra of a) ZCO and ZCO-rGO composite, b) C 1s, for ZCO-rGO composite

To deep understand the chemical composition of metals' surface in ZCO-rGO samples and the rGO conducting property, these samples were exposed to X-ray photoelectron spectroscopy (XPS). The Co $2p_{1/2}$, Co $2p_{3/2}$, O 1s, and C 1s of ZCO-rGO composite's deconvoluted spectra were confirmed in Figure 5. The ZCO-rGO survey spectrum by XPS (Figure 5 a) points out to C, Co, and O elements existence in the nanocomposite specimen. The deconvoluted spectrum of C 1s (Figure 5b) showed three distinguished crests on the rGO nanosheets at 284.2, 284.9, and 288.3 eV, corresponding to the oxygenated carbon classes that are C–C, C–O, and C=O, respectively. The highly intensity bonding of C–C indicated the respectable conducting property of rGO throughout the π electrons delocalization. On the other hand, these various bonds confirm the interaction occurrence between rGO and NCO in various ways. These bonds are hydrogen, covalent, and/or van der Waals interactions [13]. Therefore, the ZCO-rGO surface include $Zn^{3+}/^{2+}$ and $Co^{3+}/^{2+}$ couples synergetic to each other that can positively affect the processes of charging the storage [14].

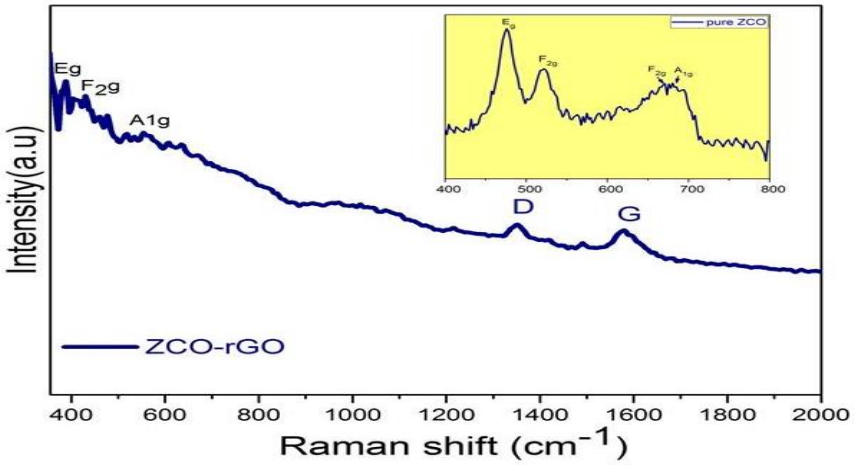


**Figure 6.** Raman spectrum of pure ZCO and ZCO-rGO.

The carbon phase nature within the composite samples can be determined efficiently by using Raman spectroscopy tool. The Raman spectra of both ZCO-rGO composite and as-prepared ZCO samples are shown in Figure 6a. The ZCO Raman fingerprints characteristics were indicated by the bands at 657, 520, and 477 $cm^{-1}$, that were almost difficult to be observed in the ZCO-rGO specimen owing to the strong signals of carbon on the surface of the composite. The carbon bands at 1512 $cm^{-1}$ (G band, the $sp_2$ hybridized carbon atoms vibration within the graphite sheets having 2D hexagonal lattice) and 1380 $cm^{-1}$ (D band, faults, and disorder within the hexagonal graphitic carbon) are strong which reveal the graphitic carbon and amorphous carbon and coexistence. The intensity ratio of the D to G band (ID/IG) is associated with the $sp_2$ domains' average size. Higher intensity ratio was obtained when the domain of $sp_2$ is smaller. The ZCO-rGO composite with high-intensity ID/IG band ratio (i.e. 0.91) implies that the presence of many defects on the rGO surface, that might be useful for getting a durable ZCO particles adhesion on the nanosheets of rGO [15]. The effective GO decreasing throughout the synthesis was resulted from the increasing D to G band ratio of NCO-rGO composite and rGO in comparison with that of GO.

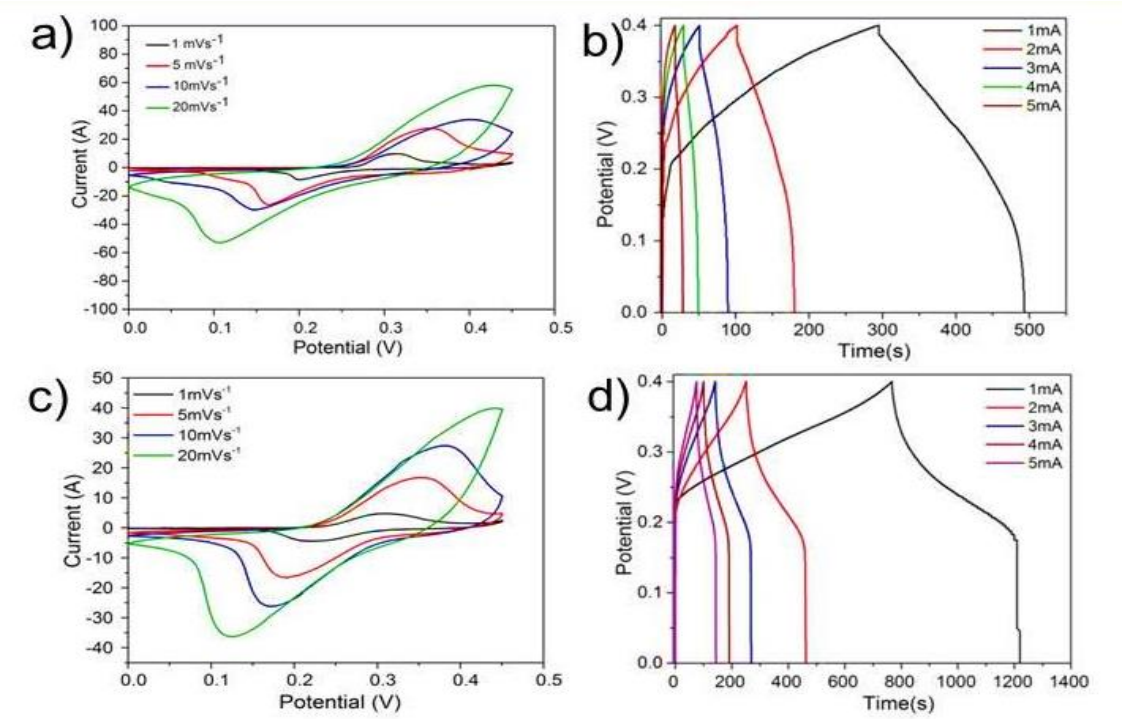


**Figure 7.** (a) CV curves at different ZCO scanning rates, (b) charging/discharging curves at different currents of ZCO, (c) CV curves at different scanning rates of ZCO- rGO, and (d) charging/discharging curves at different currents of ZCO- rGO.

The CV plots of the electrodes that consist of pristine ZCO and ZCO-rGO nanoflakes at rate of scanning equals to 10$mVs^{-1}$ within the range of potential equals to 0.0-0.45 V (vs. Hg/HgO) are shown in Figure 4.9. The ZCO-rGO composite electrode CV curves displayed specific current and integrated areas much larger than those of the electrodes made from pristine ZCO (Figure 7 (a and c)). This indicates that ZCO-rGO has an enhanced electrochemical activity and a faster process of activation. Additionally, the characteristics of the galvanostatic charge-discharge (Figure 7 (b and d)) at various specific current values were utilized for evaluating the ZCO and ZCO- rGO electrochemical performance within the range of potential equals to 0.0-

0.45 V (vs. Hg/HgO). The electrode made from ZCO-rGO, for a given current, exhibited a superior performance of charging storage and greater specific capacitance than the electrode that made from pristine ZCO as the former has higher surface area along with the enhanced electronic conductivity offered by rGO within the composite system. Figure 7a exhibits the change in the specific capacitance versus the scanning rate and the current of discharging. According to Equation (2), the ZCO-rGO specific capacitances were equal to 1022, 970, 900, and 885 $F \cdot g^{-1}$ at rates of scanning equal to 1, 5, 10 and 20 $mV.s^{-1}$, respectively. Though, the values of the specific capacitance for the electrode that made from pure ZCO at the same rates of scanning were equal to 800, 772, 710, and 688 $F \cdot g^{-1}$. These results further approved that the electrode made from ZCO-rGO had a relatively higher rate capability and capacity of storage (see Figure 8). The ZCO-rGO electrodes' specific capacitances at various currents of 1,2, 3, 4, and 5 $A.g^{-1}$, were calculated using Equation (1) to be 1200, 1188, 1112,1099 and 1023 $F \cdot g^{-1}$, respectively. Similarly, the ZCO electrodes' specific capacitances were equal to 1062, 1012, 990, 875 and 800 $F.g^{-1}$ at 1, 2, 3, 4, and 5 $A.g^{-1}$, respectively.

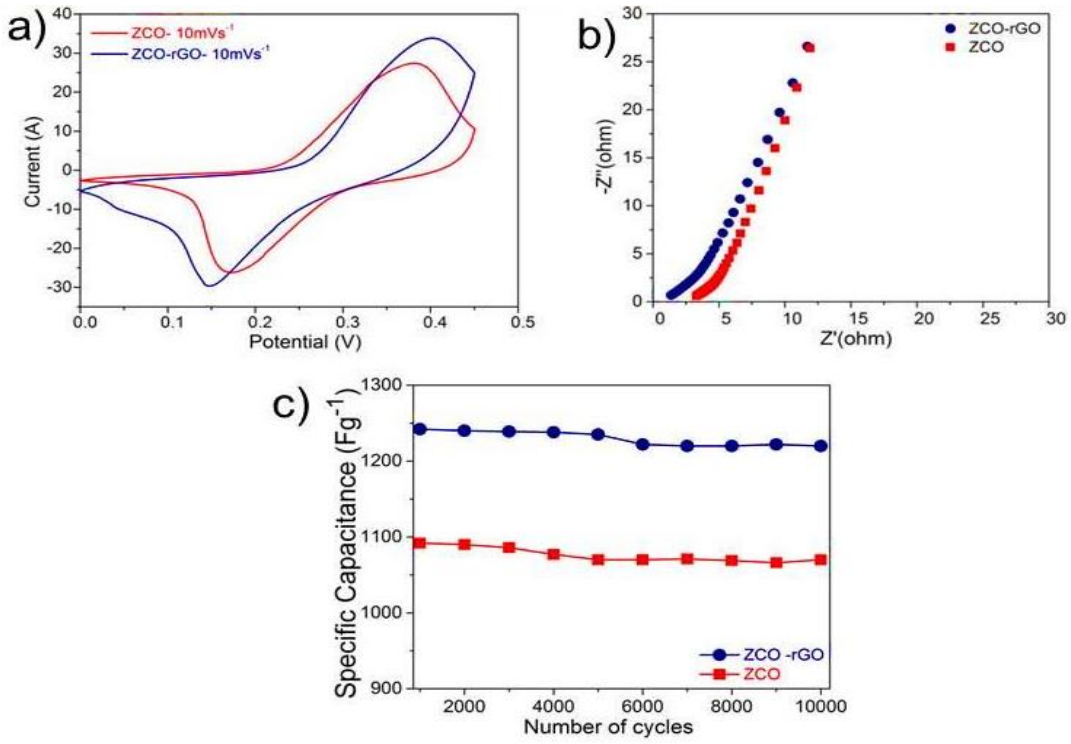


**Figure 8.** (a) CV curves of the ZCO and ZCO-rGO, (b) spectra of electrochemical impedance, and (c) ZCO and ZCO-rGO nanocomposite cycling performance.

Figure 8 shows the relationship between CVs of the ZCO nanoflakes and ZCO-rGO specific capacitance with cycles' number. According to equations (1 and 2), the specific capacitances of ZCO and ZCO-rGO samples at rate of scanning of 10 mV $s^{-1}$ were approximately equal to 1098 F $g^{-1}$ and 1242 F $g^{-1}$ f, respectively.

This finding suggests that the ZCO specific capacitance increases dramatically when graphene oxide is added to the sample. We know very well that material's electronic conductivity and morphology play a critical role in calculating the electrochemical performance. The active material's efficient application in the of nanoflakes form along with the conductivity that was provided by the reduced graphene oxide were the main reason behind improving the specific capacitance. Moreover, the improvement in the surface area of BET was an additional

parameter that led to this improvement; where, the surface areas of ZCO and ZCO-rGO were approximately equal to 65. 5$m^2$ $g^{-1}$ and 421.02$m^2$ $g^{-1}$, respectively. The larger the surface area of ZCO-rGO, the higher electrode/electrolyte interface active surface. Therefore, the ZCO flaky structure as well as the presence of the reduced graphene oxide could substantially develop the interaction between the electrolyte and electrode. For understanding the properties of the interfacial, studying the ZCO and ZCO-rGO electrochemical impedances have been carried out. As noticed in Figure 8b, Nyquist plots for ZRO and ZCO-rGO electrodes behave a semicircular form that represent the resistance of charge-transfer on the electrode interface. Whereas, the inclined line (W: Warburg impedance) within the band of low-frequency was ascribed to the diffusion of ions at the electrolyte to the electrode's interface. The first intersection with the x-axis refers to the resistance of solution (termed as Rs). The lower value of Rs in ZCO-rGO (i.e. 0.2 Ω) in comparison with that of ZCO (i.e. 1.5 Ω) was due to the ZCO-rGO electronic conductivity improvement that was provided by the rGO content. Low value of Rs is useful in increasing the performance of the power. The lower ZCO-rGO charge-transfer resistance (i.e. 0.8 Ω) than for ZCO (i.e. 2.8 Ω) reveals its lower electrochemical resistance than that of electrode made from pristine ZCO. Indeed, the electrodes' electrochemical conductivity could be increased owing to the presence of interconnected thin layers of rGO. A supercapacitor's cycle life is considered as one of the major factors in the practical applications. Figure 8c exhibits the electrodes' cycling performance tested at 2 A $g^{-1}$ of current density. The cycling stability of electrode made from ZCO-rGO is outstanding with about 92% capacitance retention over 10000 charging/discharging cycles; whereas, the electrode made from ZCO can retain only 80% of its capacitance after the same cycles. The unique architecture of ZCO-rGO nanocomposite is the main reason behind the improvement in the cycling performance as the thin layer of rGO functions as a shield on the electrode that keeps its structural integrity and increases its conductivity even with high changes in the volume throughout the charging/discharging cycles, along with obstructing the particles of ZCO from being aggregated [16].

In general, the electrode that made from ZCO-rGO composite shows high rate capability and specific capacitance and superior performance of cycling as well. These remarkable electrochemical performance could be ascribed to: (i) the rGO existence within the composite system of ZCO-rGO has improved the effective specific surface area and reduced the dispersion and migration routes for electrolyte ions; (ii) the integral and proper contact between both materials (i.e. ZCO and rGO), that led to enhance the electronic conductivity of the electrode made from composite material; and (iii) the efficient function of the rGO in the charge/discharge phase against the ZCO agglomeration [17].

**Table 1.** Electrochemical performance comparison of present system with different reported ZNC systems.

| Material | Preparation method | Specific capacitance ($Fg^{-1}$) | Capacitance retention(%) | Cycles | Reference |
|---|---|---|---|---|---|
| ZCO- Graphene | hydrothermal reaction | 143 | 93.4 | 5000 | [18] |
| ZCO-rGo | hydrothermal deposition | 139 | 6 | 5000 | [19] |
| ZCO - rGO | hydrothermal method | 110 | 2.7 | 3000 | [20] |
| ZCO - rGO | hydrothermal method | 1613 | 97.3 | 5000 | [21] |
| ZCO - Graphene | hydrothermal process | 1802 | 0 | 4000 | [22] |
| ZCO -rGO/NiO | hydrothermal method | 1256 | 80 | 3000 | [23] |
| ZCO - rGO | hydrothermal method | 626 | 99.7 | 3000 | [24] |
| ZCO - rGO | hydrothermal method | 1242 | 92 | 10000 | This work |

## 4. Conclusion

In this study, the hydrothermal method for preparing nanocomposites from ZCO and the ZCO-rGO was approved. Wrapping the hexagonal nanoflakes of ZCO with rGO sheets affect the ZCO properties in a very profound way. The results showed that composites that fabricated from ZCO-rGO have higher electrochemical properties than those made from pristine ZCO nanoflakes. The prepared ZCO-rGO composite had the ability to attain 1242 F $g^{-1}$ as the highest mean specific capacitance at 2 A $g^{-1}$ of current density and could hold about 92% of its primary capacitance after 10000 cycles of charging/discharging process. The well-connected rGO networks were the main reason behind the improvement occurred in the ZCO-rGO electrochemical performance when compared with the samples prepared from pristine ZCO. More contact between the electrolyte ions and active material surface throughout the charging/discharging process was offered by the well-connected rGO networks. Moreover, these networks could shorten the paths of electrolyte ions diffusion and provide easy accessing of electrolyte ions into the redox centres. The used method offered an easy and effective way for combining the conducting carbon-metal oxide composites with porous structures. With its outstanding electrochemical efficiency, the ZCO-rGO composite would, without any doubt, make it an attractive option for producing electrode materials with highly performance for potential energy storage applications in the future.

**Acknowledgements**

This work was supported by the University of Babylon, College of Education for Pure Sciences, Department of Physics. The equipment (SEM) used in the present study was funded by the Australian Research Council (ARC) grant LE0237478 and is located at the UOW Electron Microscopy Centre. We would also like to acknowledge the University of Wollongong for the XRD analysis. and is located at the Institute for Superconducting and Electronic Materials, University of Wollongong, Wollongong, NSW 2522, Australia.

**References**

[1]. N. G. Park et al.”Synthesis and electrochemical properties of $V_2O_5$ intercalated with binary polymers” J. Power Sources” Vol. 103, No. 2, pp. 273–279, 2002.

[2]. H. Y. Lee and J. B. Goodenough.”Supercapacitor Behavior with KCl Electrolyte” J. Solid State Chem” Vol. 144, No. 1, pp. 220–223, 1999.

[3]. B. Hussien, A. Hashim, and A. Jewad, Electrical properties of polyvinylchloride - Zinc composite, Eur. J. Soc. Sci., vol. 32, no. 2, pp. 225–229, 2012.

[4]. K. Lota, V. Khomenko, and E. Frackowiak.”Capacitance properties of poly(3,4-ethylenedioxythiophene)/carbon nanotubes composites”J. Phys. Chem. Solids” Vol. 65, No. 2–3, pp. 295–301, 2004.

[5]. B. Muthulakshmi, D. Kalpana, S. Pitchumani, and N. G. Renganathan.”Electrochemical deposition of polypyrrole for symmetric supercapacitors” J. Power Sources, Vol. 158” No. 2 SPEC. ISS., pp. 1533–1537, 2006.

[6]. T. Liangliang and J. Chunyang. ”Conducting polymers as electrode materials for supercapacitors” Prog. Chem.”Vol. 22, No. 8, pp. 1610–1618, 2010.

[7]. S. Sahoo and J. J. Shim. ”Facile Synthesis of Three-Dimensional Ternary $ZnCo_2O_4$/Reduced Graphene Oxide/NiO Composite Film on Nickel Foam for Next Generation Supercapacitor Electrodes”ACS Sustain. Chem. Eng” Vol. 5, No. 1, pp. 241–251, 2017.

[8]. M. J. Lindsay, Data analysis and anode materials for lithium ion batteries, University of Wollongong Thesis Collection, 2004.

[9]. A. N. Naveen and S. Selladurai, Novel low temperature synthesis and electrochemical characterization of mesoporous nickel cobaltite-reduced graphene oxide (RGO) composite for supercapacitor application, Electrochim. Acta, vol. 173, pp. 290–301, 2015.

[10]. W. S. Hummers and R. E. Offeman, Preparation of Graphitic Oxide, J. Am. Chem. Soc., vol. 80, no. 6, p. 1339, 1958

[11]. S. Al-Rubaye, R. Rajagopalan, S. X. Dou, and Z. Cheng, Facile synthesis of a reduced graphene oxide wrapped porous $NiCo_2O_4$ composite with superior performance as an electrode material for supercapacitors, J. Mater. Chem. A, vol. 5, no. 36, pp. 18989–18997, 2017

[12]. B. H. Rabee and A. Hashim, “Synthesis of Poly-Methyl Methacrylate-Zinc Composites and Study Electrical Properties σ,” vol. 33, no. 33, pp. 26–29, 2011.

[13]. S. AL-Rubaye, R. Rajagopalan, C.M. Subramaniyam, Z. Yu, S. X. Dou, Z. Cheng, Electrochemical performance enhancement in $MnCo_2O_4$ nanoflake/graphene nanoplatelets composite, J. Power Sources, vol. 324, pp. 179-187, 2016.

[14]. Z. Yu, Z. Cheng, Z.Tai, C.M. Subramaniyam, C. Fang, S. Al-Rubaye, X. Wang and S. Dou, Tuning the morphology of $Co_3O_4$ on Ni foam for supercapacitor application, J. RSC Adv., vol. 6, no. 51, pp. 45783-45790, 2016.

[15]. R. Rajagopalan, S. Al- Rubaye, Z. Wu, E. Wang, Y. Liu, C. Wu, W. Xiang, B. Zhong, X. Guo, S. X. Dou, H. K. Liu, A novel high voltage battery cathodes of $Fe^{2+}/Fe^{3+}$ sodium fluoro sulfate lined with carbon nanotubes for stable sodium batteries, J. Power Sources, vol. 398, pp. 175–182, 2018.

[16]. S. Sahoo and J. J Shim, Facile Synthesis of Three-Dimensional Ternary $ZnCo_2O_4$/ReducedGraphene Oxide/NiO Composite Film on Nickel Foam for NextGeneration Supercapacitor Electrodes, J. ACS Sustainable Chem. Eng., vol. 5, no. 1, pp. 241−251, 2017.

[17]. S. AL- Rubaye ,R. Rajagopalan ,Electrochemical Performance Evaluation of Ni foam $NiCo_2O_4$-CNTs for Energy Storage Applications, J. Test &Engineering management, vol. 83,pp. 12828-12841,2020.

[18]. I. K. Moon, S. Yoon, and J. Oh, "Mesoporous ZnCo 2 O 4 Nanowires Grown on Graphene / Sponge Foam for High Performance Flexible All-Solid- State Supercapacitors."

[19]. Z. Gao *et al.*, "ZnCo 2 O 4 -reduced graphene oxide composite with balanced capacitive performance in asymmetric supercapacitors," *Appl. Surf. Sci.*, vol. 442, pp. 138–147, 2018, doi: 10.1016/j.apsusc.2018.02.152.

[20]. J. Qi *et al.*, "Facile synthesis of mesoporous ZnCo2O4 nanosheet arrays grown on rGO as binder-free electrode for high-performance asymmetric supercapacitor," *J. Mater. Sci.*, vol. 53, no. 23, pp. 16074–16085, 2018, doi: 10.1007/s10853-018-2757-7.

[21]. S. Sahoo and J. J. Shim, "Nanostructured 3D zinc cobaltite/nitrogen-doped reduced graphene oxide composite electrode for supercapacitor applications," *J. Ind. Eng. Chem.*, vol. 54, pp. 205–217, 2017, doi: 10.1016/j.jiec.2017.05.035.

[22]. W. Bai *et al.*, "Preparation of ZnCo2O4 nanoflowers on a 3D carbon nanotube/nitrogen-doped graphene film and its electrochemical capacitance," *J. Mater. Chem. A*, vol. 3, no. 43, pp. 21891–21898, 2015, doi: 10.1039/c5ta05798a.

[23].S. Sahoo and J. J. Shim, "Facile Synthesis of Three-Dimensional Ternary ZnCo2O4/Reduced Graphene Oxide/NiO Composite Film on Nickel Foam for Next Generation Supercapacitor Electrodes," *ACS Sustain. Chem. Eng.*, vol. 5, no. 1, pp. 241–251, 2017, doi: 10.1021/acssuschemeng.6b01367.

[24]. Y. Wang *et al.*, "Growth of zinc cobaltate nanoparticles and nanorods on reduced graphene oxide porous networks toward high-performance supercapacitor electrodes," *J. Alloys Compd.*, vol. 668, pp. 1–7, 2016, doi: 10.1016/j.jallcom.2016.01.212.